Identification of Two Distinct Hybrid State Intermediates On the Ribosome

James B. Munro, Roger B. Altman, Nathan O'Connor, and Scott C. Blanchard
Department of Physiology and Biophysics
Weill Medical College of Cornell University

SUPPLEMENTAL MATERIALS

Wild-type[1]	τ_C	τ_{H1}	τ_{H2}
fMet-Phe	59.5±1.7	18.6±1.2	21.9±1.3
Met-Phe	60.9±2.2	18.3±1.5	20.8±1.6
Phe	72.1±1.2	13.0±0.80	14.9±0.98
Laboratory Strains			
fMet-Phe[2]	52.9±1.6	21.6±1.1	25.5±1.3
ΔL1[3,4]	73.4±1.6	11.6±0.97	15.0±1.3
G2252C[2,4]	17.4±1.2	28.0±1.2	54.7±1.6
G2553C[2,4]	19.8±1.4	43.1±1.7	37.1±1.7

[1] Ribosomes isolated from *E. coli* MRE600.
[2] Ribosomes isolated from *E. coli* DH10 as described (Dorner et al., 2006).
[3] Ribosomes isolated from *E. coli* BL21(DE3).
[4] Contain fMet-Phe-tRNA^{Phe} in the A site.

Supplemental Table 1. The percentage of time spent in the classical state, hybrid state 1, and hybrid state 2 shows the shift in equilibrium upon changing the composition of the peptide and mutating the ribosome. Values are represented as an average ± standard error.

FRET Values of tRNA Configurations

Wild-type[1]	Classical state	Hybrid state-1	Hybrid state-2
fMet-Phe	0.55±0.04	0.39±0.03	0.24±0.03
Met-Phe	0.56±0.04	0.39±0.04	0.23±0.03
Phe	0.56±0.04	0.38±0.03	0.23±0.04
Laboratory Strains			
fMet-Phe[2]	0.56±0.05	0.37±0.06	0.25±0.05
ΔL1[3,4]	0.57±0.04	0.40±0.03	0.24±0.04
G2252C[2,4]	0.53±0.04	0.36±0.03	0.21±0.03
G2553C[2,4]	0.52±0.05	0.34±0.03	0.21±0.03

[1] Ribosomes isolated from *E. coli* MRE600.
[2] Ribosomes isolated from *E. coli* DH10 as described (Dorner et al., 2006).
[3] Ribosomes isolated from *E. coli* BL21(DE3).
[4] Contain fMet-Phe-tRNA^{Phe} in the A site.

Supplemental Table 2. All points in the single-molecule trajectories assigned through idealization in QuB to a unique state were used to estimate each state's apparent FRET value. Values are represented as an average ± standard deviation.

Apparent Transition Rates (All Molecules)

Wild-type[1]	$k_{C\rightarrow H1}$	$k_{H1\rightarrow C}$	$k_{H1\rightarrow H2}$	$k_{H2\rightarrow H1}$	$k_{C\rightarrow H2}$	$k_{H2\rightarrow C}$
fMet-Phe	1.48±0.14	4.32±0.25	4.07±0.22	2.77±0.16	1.28±0.11	3.91±0.26
Met-Phe	1.50±0.15	5.57±0.38	5.00±0.28	3.82±0.25	1.19±0.14	3.73±0.25
Phe	1.02±0.07	5.11±0.25	3.92±0.21	2.72±0.17	0.80±0.06	3.50±0.22
Laboratory Strains						
fMet-Phe[2]	1.70±0.10	4.60±0.27	4.02±0.22	2.85±0.19	1.34±0.11	2.67±0.20
ΔL1[3,4]	1.12±0.10	5.98±0.34	4.50±0.31	2.62±0.19	0.77±0.07	4.14±0.33
G2252C[2,4]	3.10±0.23	1.58±0.20	5.53±0.37	3.21±0.24	2.72±0.26	0.83±0.16
G2553C[2,4]	4.58±0.38	2.10±0.26	3.92±0.35	3.54±0.31	2.19±0.23	1.16±0.20

[1] Ribosomes isolated from *E. coli* MRE600.
[2] Ribosomes isolated from *E. coli* DH10 as described (Dorner et al., 2006).
[3] Ribosomes isolated from *E. coli* BL21(DE3).
[4] Contain fMet-Phe-tRNA^{Phe} in the A site.

Supplemental Table 3. Rate constants are shown for transitions between each FRET state shown in **Figure 5** considering all molecules detected in each experimental system. Rate constants were calculated by averaging those derived from maximization-likelihood optimization of each trace in QuB. Data from wild-type complexes are labeled according to the peptide or amino acid on the A-site tRNA. Subscripts *C*, *H1*, and *H2* refer to classical state, hybrid state-1, and hybrid state-2, respectively. Rate constants are given in units of sec^{-1}, and represented as an average ± standard error.

Relative Distance Changes of tRNA

Wild-type[1]	$\Delta R_{C1 \leftrightarrow H1}$	$\Delta R_{C1 \leftrightarrow H2}$	$\Delta R_{H1 \leftrightarrow H2}$
fMet-Phe	6.62	14.7	8.06
Met-Phe	7.01	15.7	8.74
Phe	7.46	15.7	8.28
Laboratory Strains			
fMet-Phe[2]	6.61	14.4	6.49
ΔL1[3,4]	6.95	15.5	8.51
G2252C[2,4]	7.23	16.0	8.79
G2553C[2,4]	7.81	15.6	7.81

[1] Ribosomes isolated from *E. coli* MRE600.
[2] Ribosomes isolated from *E. coli* DH10 as described (Dorner et al., 2006).
[3] Ribosomes isolated from *E. coli* BL21(DE3).
[4] Contain fMet-Phe-$tRNA^{Phe}$ in the A site.

Supplemental Table 4. Based on a Förster distance of 60Å for the Cy3/Cy5 dye pair, approximate changes in the intermolecular distance between tRNA were estimated for each change in FRET shown in Supplemental Table 3. Distances are given in Angstroms.

Supplemental Figure 1. The histogram of experimental FRET traces obtained for wild-type complexes (A) is well reproduced by simulation of a 5-state kinetic model (B), which contains 2 hybrid states. Simulated data from the 4-state model (C), having only one hybrid state, has a notable lack of FRET signal in the intermediate region. (D) The one-dimensional histogram is well fit by a sum of four Gaussians (individually in red; the sum in black). Simulated histograms from the 5-state (blue) and 4-state (pink) models are overlaid for comparison.

Supplemental Figure 2. (A) SDS-PAGE analysis of ribosomal proteins isolated from wild-type and L1-knock-out (Δ*rpla)* strains showing the absence of a specific band corresponding to L1. (B) Growth curves of wild-type (black squares) and the Δ*rpla* strain (red circles) showing a severe growth deficiency of the mutant strain.

Supplemental Figure 3. Cy3-Met-tRNA^{fMet} in the P site reacts rapidly with 2mM puromycin (green triangles). The rate of reaction fits a triple exponential ($A_1e^{-k1t}+A_2e^{-k2t}+A_3e^{-k3t}$). Holding the photobleaching rate constant (0.40/sec) (pink triangles), the reaction rates are estimated at: (wild-type); k_2=4.74/sec, k_3=0.015/sec (G2552C); k_2=0.31/sec, k_3=0.04/sec, and (G2553); k_2=11/sec, k_3=0.2/sec. The rate of peptidyl-tRNA drop off from the A site, insignificant at 15mM Mg^{2+} (blue circles), is estimated by fitting the loss of Cy3 fluorescence in the absence of puromycin to a double exponential decay ($A_1e^{-k1t} + A_2e^{-k2t}$). By holding the photobleaching rate constant (0.40/sec), the peptidyl-tRNA drop off rate is estimated at: (wild-type) k_2=0.15/sec; (G2552C) k_2=0.012/sec; and (G2553) k_2=0.20/sec. Puromycin reactivity of A-site peptidyl-tRNA is

estimated by fitting each data set to a triple exponential, holding the determined photobleaching and drop off rates constant. The data (red squares, and **Figure 4**) show that the puromycin reaction rates are: (wild-type) A3=22%, k_3=0.81/sec; (G2252C) A3=8%, k_3=0.036/sec*; (G2553C) A3*=36%, τ_3=0.53/sec. All fits achieve an $R^2 > 0.9$.

Supplemental Figure 4. As described in the text, in order to arrive at a more accurate representation of the underlying dynamics, a subpopulation of FRET traces that visited all three states (classical state, hybrid state 1, and hybrid state 2) were selected for kinetic analysis from those represented in **Figure 2**. Data are presented in the same format as **Figure 2**. The simulated data in the bottom row of panels was generated from the average rate constants in Supplemental Table 3.

Supplemental Figure 5. As described in the text, in order to arrive at a more accurate representation of the underlying dynamics, a subpopulation of FRET traces that visited all three states (classical state, hybrid state 1, and hybrid state 2) were selected for kinetic analysis from those represented in **Figure 3**. Data are presented in the same format as **Figure 3**. The simulated data in the bottom row of panels was generated from the rate constants in Supplemental Table 3.

Supplemental Figure 6. Ribosome complexes from two different wild-type *E. coli* strains display slightly different dynamics. The left column of panels displays data on ribosome complexes from MRE600. The right column of panels shows data from DH10-derived wild-type ribosomes containing the MS2 binding element, the strain from which

the G2252C and G2553C mutant ribosomes were purified in this work (Youngman and Green, 2005; Dorner et al., 2006). As seen in the histograms, as well as **Table 1** and Supplemental Table 3, the kinetics of wild-type DH10 ribosomes are characterized by slightly greater stability in hybrid state 2, and thus a slower rate of locking. This is also reflected by the slightly smaller number of transitions per trace.

In addition to these sets of data being from ribosomes from different strains, they were purified by different methods. The wild-type, G2252C, and G2553C DH10 ribosomes were isolated by an affinity purification method whereby the 23S rRNA is tagged with an RNA stem-loop which binds specifically to the coat protein of the MS2 bacteriophage. The ribosomes are purified over a column with the coat protein fused to glutathione S-transferase, and immobilized to a glutathione matrix (Youngman and Green, 2005). The differences observed between the two wild-type complexes cannot be attributed to the presence of different amounts of E-site tRNA as single-molecule FRET data were also collected on ribosome complexes which were formed from isolated 30S and 50S ribosomal subunits from MRE600. These complexes did not show any appreciable difference in behavior from the MRE600 complexes formed using tight-coupled 70S ribosomes (data not shown).

Generation of an *E. coli* Δ*rpla* Strain

E. coli BL21(DE3), Δ*rpla* was generated by a gene gorging protocol (Herring et al., 2003). *rplA* was cloned into the pCR-Blunt II-TOPO vector (Invitrogen) by megaprimer PCR (Xu et al., 2003) with residue A84 mutated to a TAG amber stop codon. The plasmid containing genes coding for λ-Red recombinase and the mega-

nuclease I-Sce I were obtained from Scarab Genomics. Although not required for cell survival (Subramanian and Dabbs, 1980), cells lacking L1 showed a significant growth defect as compared to wild-type (Supplemental Figure 2B). Removal of *rplA* from the ribosome, suggested by a strong growth defect, was verified by SDS-PAGE analysis of extracted ribosomal proteins (Supplemental Figure 2).

Aminoacylation and Fluorescent Labeling of tRNA

Pure $tRNA^{fMet}$ and $tRNA^{Phe}$ from *E. coli* MRE600 were purchased (Sigma). Aminoacylation, formylation, and fluorescent labeling of tRNA were performed as previously described (Blanchard et al., 2004a-b). Charging of $tRNA^{Phe}$ was achieved using recombinant phenylalanyl tRNA synthetase (PheRS) cloned into the pET-SUMO vector (Invitrogen), overexpressed, and purified over Ni-NTA agarose column (Qiagen) where the 6-Histidine-SUMO tag was removed by prior digestion with SUMO protease (Invitrogen). The efficiency of aminoacylation and dye labeling were verified by FPLC using a TSK Phenyl 5PW column (TOSOH Bioscience).

Preparation of Ribosome Complexes, tRNA, and Translation Factors

Wild-type and mutant tight-coupled 70S ribosomes were initiated on purified 5'-biotinylated gene 32-derived mRNA (5'-biotin-CAA CCU AAA ACU UAC ACA CCC UUA GAG GGA CAA UCG AUG UUC AAA GUC UUC AAA GUC AUC) (Dharmacon). Bacterial Initiation Factors used in the preparation of initiation complexes were cloned and purified as described for EFs Tu, Ts, and G (Blanchard et al., 2004a).

Phenylalanyl tRNA synthetase (PheRS) was cloned into the pET-SUMO vector (Invitrogen), overexpressed, and purified to homogeneity on a Ni-NTA agarose column (Qiagen). The N-terminal 6-Histidine-SUMO tag was removed by proteolytic cleavage with SUMO protease. $tRNA^{Phe}$(Cy5-acp^3U47) was FPLC purified and aminoacylated *in situ* to avoid deacylation during purification. The aminoacylation reaction of $tRNA^{Phe}$ was carried out by reaction of 1μM $tRNA^{Phe}$(Cy5-acp^3U47), 1mM L-phenylalanine, and 0.6μM PheRS, in a buffer of 50mM Tris-HCl, pH 8, 20mM KCl, 100mM NH_4Cl, 10mM $MgCl_2$, 1mM DTT, 2.5mM ATP, and 0.5mM EDTA incubated for 10min at 37°C. Ternary complex of EF-Tu(GTP)-Phe-$tRNA^{Phe}$(Cy5-acp^3U47) was prepared by adding to the aminoacylation reaction 5.8μM EF-Tu, 1mM GTP, 3.7μg/ml pyruvate kinase, 7μg/ml myokinase, and 3mM phosphoenolpyruvate, and incubating for an additional 5min at 37°C.

All single-molecule experiments were conducted in standard Tris-Polymix buffer containing 50mM Tris Acetate, pH 7.5, 15mM MgOAc, 100mM KCl, 5mM NH_4OAc, 0.5mM $CaCl_2$, 0.1mM EDTA, 5mM putrescine, and 1mM spermidine. The EF-Tu(GTP)-Phe-$tRNA^{Phe}$(Cy5-acp^3U47) formation reaction was diluted to 50nM Phe-$tRNA^{Phe}$(Cy5-acp^3U47) in Tris-Polymix buffer and delivered to surface-immobilized initiation complexes. After incubating for 1min at room temperature, ternary was rinsed out of the reaction chamber with Tris-Polymix buffer.

Details of Kinetic Analysis

Single-molecule fluorescence trajectories were identified and extracted from multiple wild-field movies by custom-made Matlab programs according to four criteria:

(1) the mean total fluorescence intensity (I_{Cy5}+I_{Cy3}) exceeded a predetermined threshold; (2) the lifetime of Cy3 fluorescence lasted more than 1sec; (3) at any point during the trace, FRET efficiency was greater than 0.1; and (4) fluorescence correlation coefficients were ≤0.2 or ≥0.2. The histograms in all Figures were compiled in Matlab from the first 2 seconds of each FRET trace, and plotted in Origin. FRET traces were imported into QuB and the first 400 frames (16sec) of each trace were idealized to Markov chain models by a segmental k-means algorithm (Qin, 2004). The FRET amplitudes, standard deviations, and initial probabilities of the model states were obtained by analysis of the histograms in **Figures 2B** and **3B**. The quality of idealization was evaluated by visual inspection, and comparison with the underlying fluorescence traces. In a small population of FRET traces (~5%) poor idealization was obtained due to FRET amplitudes that fell sufficiently far from the mean values input into the Markov model. These trajectories were eliminated from further analysis.

The sequence of dwell times from the idealization of the remaining traces was used for fitting of the Markov chain by a maximum likelihood estimation procedure (Qin et al., 1996, 1997). In all cases, the criteria for model convergence were set at 0.001 for the log-likelihood, and 0.01 for the gradient of the log-likelihood. The traces from wild-type MRE600 ribosome complexes were fit to two different Markov models: one containing a single hybrid state, and the second containing both hybrid states 1 and 2. The maximized log-likelihood per transition from all traces were summed together and corrected for the two models having different numbers of parameters by the Akaike information criterion (AIC) (Akaike, 1974). The relative AIC values, 869.2 for the model with two hybrid states, and 1580.2 for the model with one hybrid state, confirmed that the

data is better fit by the model with two hybrid states. The optimized kinetic parameters from each trace were averaged to form a single model. Simulated single-molecule FRET traces were generated in QuB from the average optimized model, and compiled into histograms as for the experimental data.

To verify that hybrid states 1 and 2 were distinct FRET states, and not a continuum of FRET values, transition density plots were constructed from the idealized data. As described by McKinney et al. (2006), these plots are constructed by compiling a 2-dimensional histogram of FRET values before and after each transition. The resulting peaks shown in **Figures 2** and **3**, and Supplemental Figures 4 and 5, indicate the relative frequency of each transition, and verify that hybrid states 1 and 2 are distinct FRET states.

Derivation of $k_{locking}$ and $k_{A/P}$

The complete 5-state model of tRNA dynamics on the ribosome is shown at right, which includes the 3 states shown in **Figure 5**, as well as the photobleached (*PB*) and blinking (*B*) states. For both $k_{locking}$ and $k_{A/P}$ we want to calculate the rate of transition from two states in dynamic exchange into a single state. The process for determining such a rate is outlined below for $k_{locking}$, and is identical for $k_{A/P}$. Both are special cases of the more general procedure demonstrated by

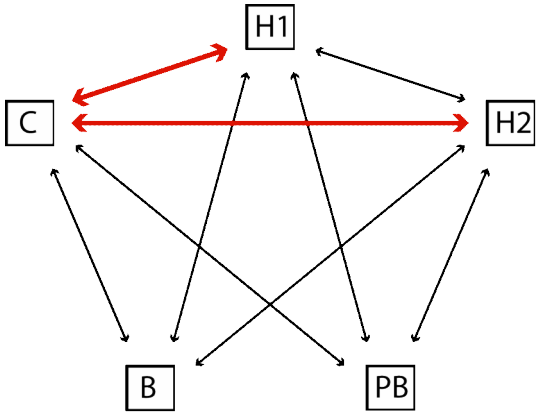

Supplemental Figure 7. Complete kinetic model considered, describing tRNA dynamics on the ribosome. Highlighted in red are the transitions combined to calculate $k_{locking}$.

Colquhoun and Hawkes (1981). Due to the minimal blinking rate we have neglected to exchange between *H1* and *H2*, and *B*.

We seek to determine the probability density function (PDF) describing transitions out of a set of 2 connected states (*H1* and *H2*) into a single state (*C*),

$$f_{H\to C}(t) = w_1 \exp(-\kappa_1 t) + w_2 \exp(-\kappa_2 t),$$

where w_1 and w_2 are normalization constants, and k_1 and k_2 are time constants determined below. The master equation expressing the probability $P_{i\to C}(t)$ of the system being found in the classical state at time t, given that it began in *H1* or *H2* at $t=0$ in terms of the transition rates between states is

$$\frac{dP_{i\to C}(t)}{dt} = P_{i\to H1}(t)k_{H1\to C} + P_{i\to H2}(t)k_{H2\to C},$$

where i is either *H1* or *H2*. The quantity $dP_{i\to C}(t)/dt$ is the probability density of transitions from i to C. We therefore need to obtain the transition probabilities $P_{i\to H1}(t)$ and $P_{i\to H2}(t)$. This is most easily done by combining these probabilities into the 2×2 matrix $\mathbf{P}_{HH}$, and noting that they satisfy analogous master equations, which are expressed in matrix notation as

$$\frac{d\mathbf{P}_{HH}(t)}{dt} = \mathbf{P}_{HH}(t)\mathbf{K}_{HH}, \tag{1}$$

where $\mathbf{K}_{HH}$ is the matrix of transition rates between hybrid states 1 and 2,

$$\mathbf{K}_{HH} = \begin{pmatrix} k_{H1\to H1} & k_{H1\to H2} \\ k_{H2\to H1} & k_{H2\to H2} \end{pmatrix},$$

which is a submatrix of the complete 5×5 matrix of transition rates, **K**. The diagonal elements of **K** (and of $\mathbf{K}_{HH}$) are defined such that the rows of **K** sum to zero. Using standard matrix methods, $\mathbf{P}_{HH}(t)$ may be obtained from the spectral decomposition of

$$\mathbf{P}_{HH}(t) = \mathbf{A}_1 \exp(\lambda_1 t) + \mathbf{A}_2 \exp(\lambda_2 t)$$

$\mathbf{K}_{HH}$. For this we calculate the eigenvalues $\lambda_{1,2}$ and eigenvectors $\mathbf{v}_{1,2}$ of $\mathbf{K}_{HH}$, which are readily obtained analytically, or numerically in Matlab (e.g.). We can then express the solutions to (1) as

where $\mathbf{A}_{1,2}$ are obtained from the eigenvectors of $\mathbf{K}_{HH}$. These equations are then inserted into $dP_{i\rightarrow C}(t)/dt$. As there are two hybrid states in our model (i.e. $i=H1,H2$),

$$f_{H\rightarrow C}(t) = \pi_{H1}\frac{dP_{H1\rightarrow C}(t)}{dt} + \pi_{H2}\frac{dP_{H2\rightarrow C}(t)}{dt},$$

where π_{H1} and π_{H2} are the relative probabilities of the system beginning in *H1* and *H2* at $t=0$, respectively.

We can then define $k_{locking}$ as the average rate of transition from the hybrid states to the classical state,

$$\frac{1}{k_{locking}} \equiv < t > = \int_0^\infty t f_{H\rightarrow C}(t)dt,$$

so that

$$k_{A/P}, k_{locking} = \frac{\lambda_1^2\lambda_2^2}{w_1\lambda_2^2 + w_2\lambda_1^2}.$$

REFERNCES

Akaike, H. (1974). A New Look at Statistical Model Identification. IEEE Trans. Auto. Cont. *19*, 716-723.

Blanchard, S.C., Kim, H.D., Gonzalez, R.L., Puglisis, J.D., and Chu, S. (2004a). tRNA dynamics on the ribosome during translation. Proc. Natl. Acad. Sci. USA *101*, 12893-12898.

Colquhoun, D., and Hawkes, A.G. (1981). On the stochastic properties of single ion channels. Proc. R. Soc. Lond. B *211*, 205-235.

Dorner, S., Brunelle, J., Sharma, D., and Green, R. (2006). The hybrid state of tRNA is an authentic translation elongation intermediate. Nat. Struct. Mol. Biol. *13*, 234-241.

McKinney, S.A., Joo, C., and Ha, T. (2006). Analysis of Single-Molecule FRET Trajectories Using Hidden Markov Modeling. Biophys. J. *91*, 1941-1951.

Qin, F., Auerbach, A., and Sachs, F. (1996). Estimating Single-Channel Kinetic Parameters from Idealized Patch-Clamp Data Containing Missed Events. Biophys. J. *70*, 264-280.

Qin, F., Auerbach, A., and Sachs, F. (1997). Maximum likelihood estmation of aggregated Markov processes. Proc. R. Soc. Lond. B. *264*, 375-383.

Qin, F. (2004). Restoration of Single-Channel Currents Using the Segmental k-Means Method Based on Hidden Markov Modeling. Biophys. J. *86*, 1488-1501.

Subramanian, A.R., and Dabbs, E.R. (1980). Functional studies on ribosomes lacking protein L1 from mutant *Escherichia coli*. Eur. J. Biochem. *112*, 425-430.

Youngman, E.M., and Green, R. (2005). Affinity purification of in-vivo-assembled ribosomes for in vitro biochemical analysis. Methods *36*, 305-312.

Supplemental Figure 1

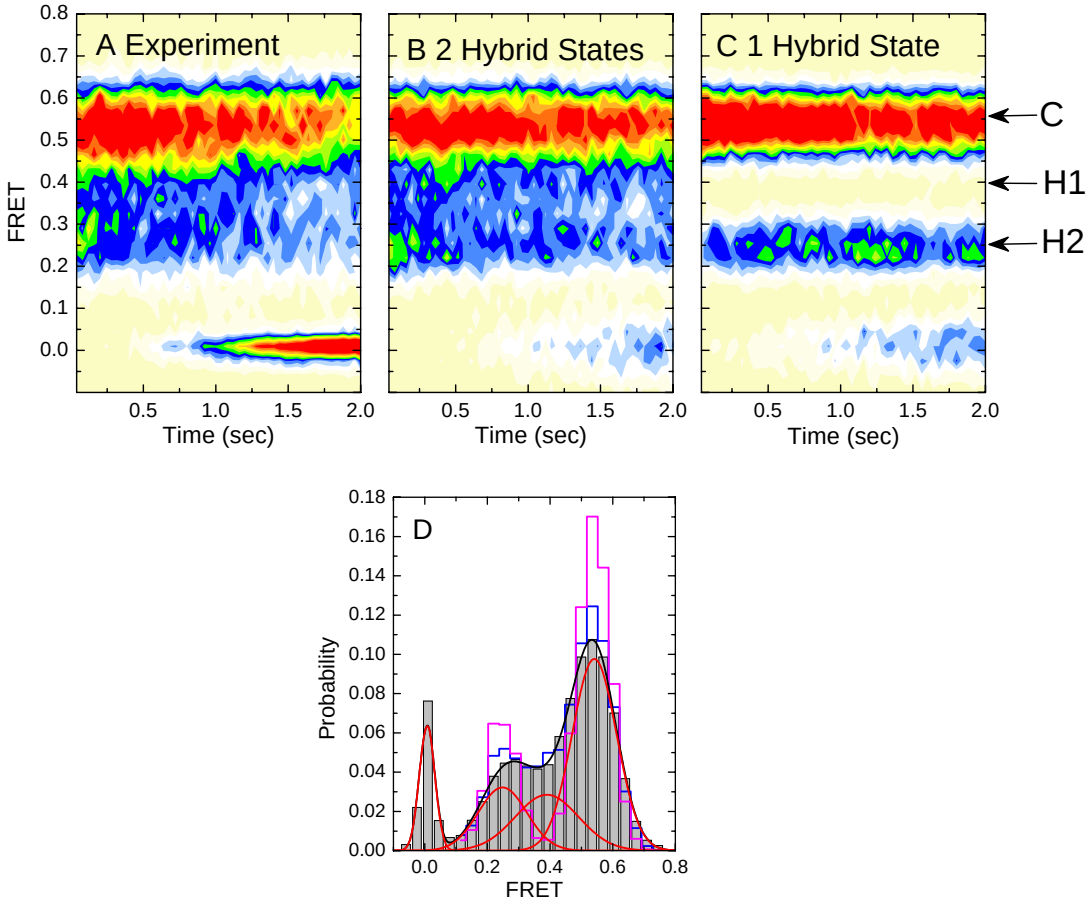

Supplemental Figure 2

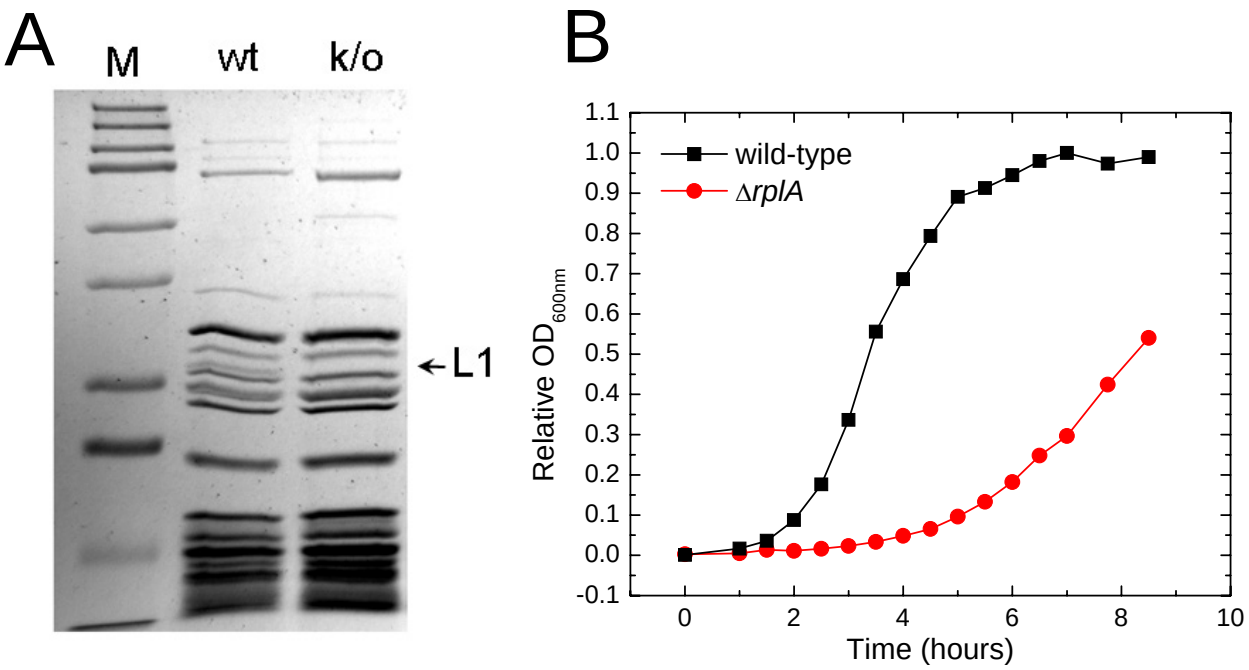

F) Supplemental Figure 3

Supplemental Figure 3

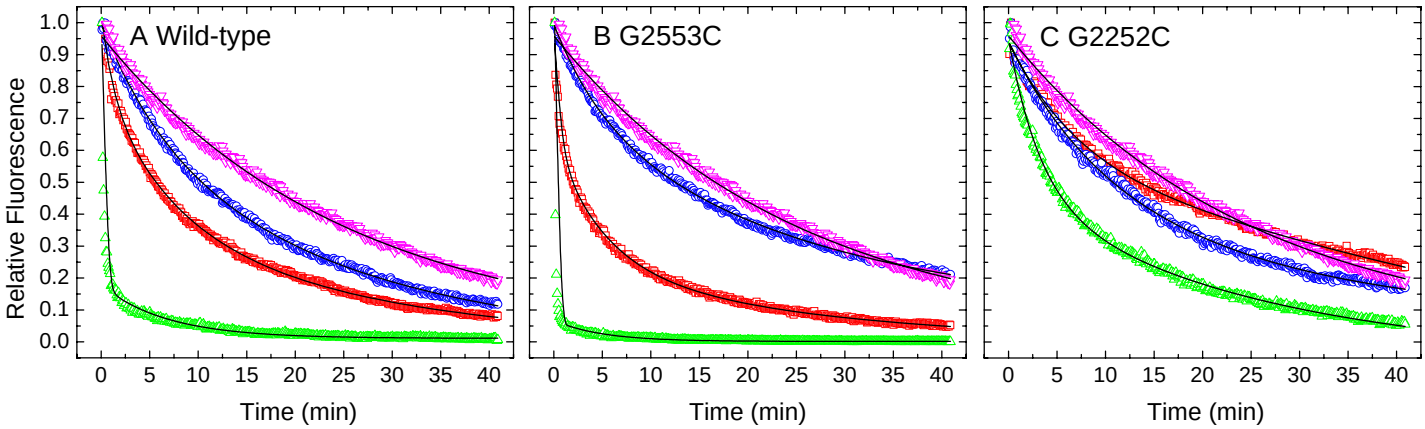

F) Supplemental Figure 4

Supplemental Figure 4

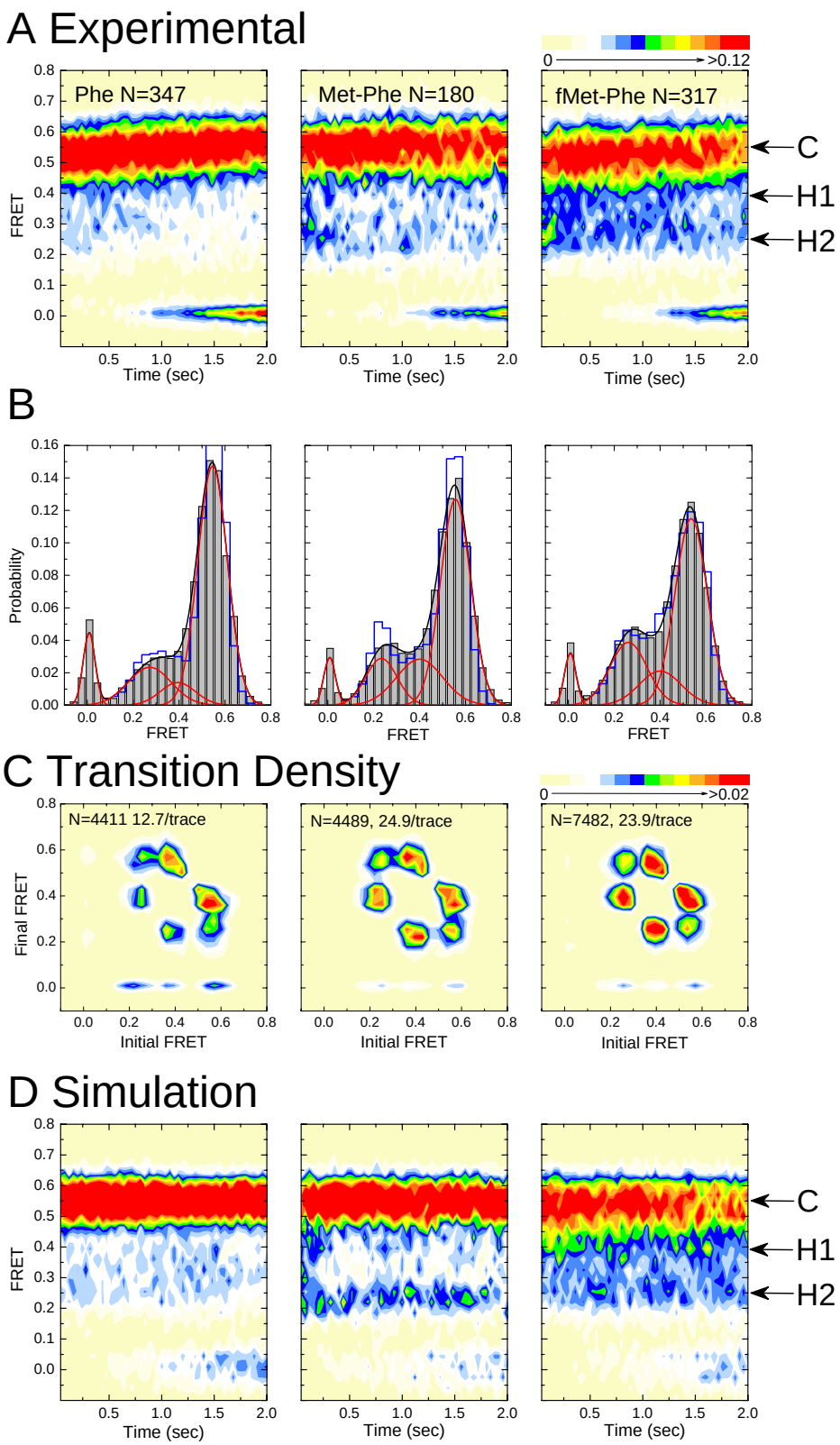

Supplemental Figure 5

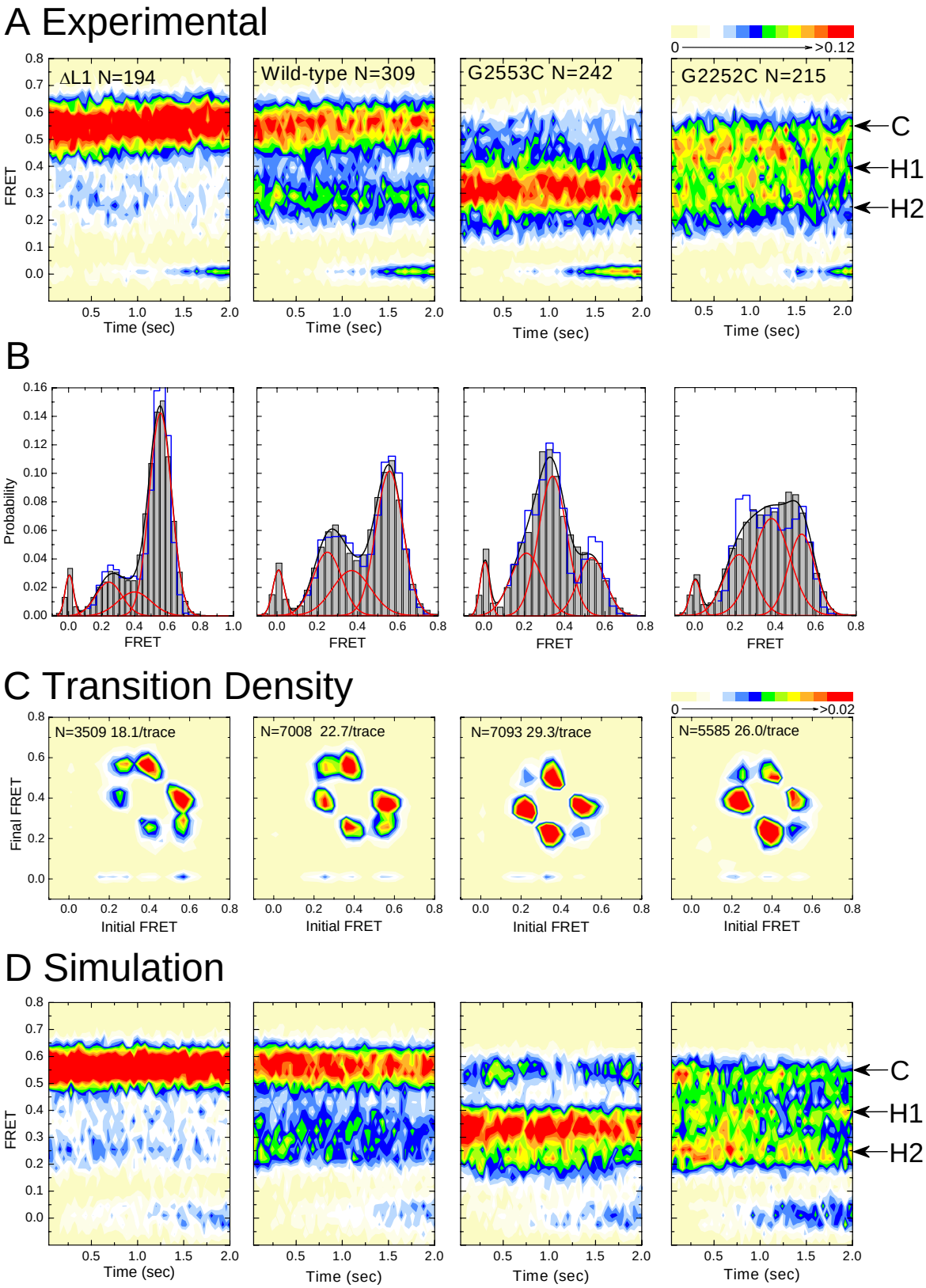

F) Supplemental Figure 6

Supplemental Figure 6